

# Core Temperature Estimation for Self-Heating Automotive Lithium-Ion Batteries in Cold Climates

Chong Zhu , Member, IEEE, Yunlong Shang , Member, IEEE, Fei Lu , Member, IEEE, Yan Jiang , Chenwen Cheng , and Chris Mi , Fellow, IEEE

## I. INTRODUCTION

**Abstract**—The onboard battery self-heaters are employed to improve the performance and lifetime of the automotive lithium-ion batteries under cold climates. The battery performance is determined by the core temperature which is significantly higher than the surface temperature during the fast self-heating, while only the surface temperature can be directly measured. By estimating the core temperature to monitor the self-heating condition, the heating time and the energy consumption can be improved. However, the high-frequency heating current and the time-variant battery impedance cannot be measured in real time by a low-sampling-rate battery management system, so that the regular core temperature estimation methods are not applicable during the self-heating. To solve the issues, an online core temperature estimation algorithm based on the lumped thermal–electrical model is developed for the onboard ac self-heater. By implementing an extended state observer to compensate for the effect of the parameter uncertainties, the core temperature can be accurately detected even with the unknown internal resistance and root mean square (RMS) heating current. The experimental validation of 18 650 lithium-ion batteries shows that the core temperature estimation error is within only 1.2 °C. As a result, the self-heating time and energy consumption can be reduced by 50%.

**Index Terms**—Battery self-heater, core temperature estimation, electric vehicles (EVs), energy saving, extended state observer (ESO).

Manuscript received May 29, 2019; revised November 3, 2019; accepted December 6, 2019. Date of publication December 23, 2019; date of current version February 6, 2020. This work was supported by the U.S. Department of Energy (DOE) through the ARPA-E NEXTCAR Program under Award DE-AR0000797. Paper no. TII-19-2107. (Corresponding authors: Yunlong Shang; Chris Mi.)

C. Zhu is with the School of Mechanical Engineering, Shanghai Jiao Tong University, Shanghai 200240, China (e-mail: chong.zhu@sjtu.edu.cn).

Y. Shang is with the School of Control Science and Engineering, Shandong University, Jinan 250100, China (e-mail: yshang@sdu.edu.cn).

F. Lu is with the Department of Electrical and Computer Engineering, Drexel University, Philadelphia, PA 19104 USA (e-mail: fei.lu@drexel.edu).

Y. Jiang is with the School of Electrical Engineering, Beijing Jiaotong University, Beijing 100044, China (e-mail: yanj@bjtu.edu.cn).

C. Cheng and C. Mi are with the Department of Electrical and Computer Engineering, San Diego State University, San Diego, CA 92182 USA (e-mail: chenwen.cheng@sdsu.edu; mi@ieee.org).

Color versions of one or more of the figures in this article are available online at <http://ieeexplore.ieee.org>.

Digital Object Identifier 10.1109/TII.2019.2960833

THE lithium-ion batteries have been widely used in electric vehicles (EVs) for their high specific energy and power density. However, thermal issues of lithium-ion batteries are often criticized as the main concern of energy storage failure and degradation [1]. Especially, in cold climates, the lithium-ion batteries suffer severe loss of energy and power, resulting in the dramatically reduced driving range of EVs [2]. In order to alleviate the “range anxiety” in cold climates, it is essential to preheat the batteries to a suitable temperature for EV driving in cold weather [3].

Various preheating methods have been developed for automotive lithium-ion batteries to improve poor performance at low temperatures [3]–[13]. Among the different heating methods, the internal heating methods utilize the ac to generate heat from inside of the battery itself, avoiding the long paths of heat conduction and the local hot spots near the heating sources [6]–[13]. Therefore, compared to the external heating methods, the internal heating can provide a faster speed, higher efficiency, and more uniform temperature distribution. Moreover, the battery self-heater presented in [11] and [12] utilizes the battery energy for preheating without external power supplies, providing flexible applicability for EVs in different parking areas.

In practice, only the surface temperature is measurable for automotive battery cells. In the preheating application, the self-heater stops heating the batteries when the measured surface temperature reaches the acceptable values for driving, e.g., 0–5 °C. However, compared to the surface temperature, the core temperature is more relevant to battery performance, such as the available power and capacity. Due to the continuously high charge/discharge current during the preheating, there is a significant temperature difference between the surface and the core, e.g., 10 °C or more [14]. Thus, it consumes more electrical energy and heating time to raise the battery surface temperature to the threshold value, leading to the additional driving range reduction in winter. On the contrary, if the battery core is not sufficiently heated, the degraded battery power and capacity also deteriorate the EV range in cold climates. Consequently, the core temperature monitoring is crucial for the battery self-heating, which is beneficial to extend the driving range in cold weather.

In previous works, the core temperature estimation methods are developed for battery state monitoring. The most common

approach is the electrochemical-impedance-spectroscopy (EIS) measurement-based method [14]–[18]. As the battery impedance closely depends on the core temperature, studies [18]–[20] show that the EIS measurement is applied to estimate the core temperature and other health-related parameters, providing satisfying accuracy. However, the impedance–temperature characteristic should be acquired in advance through tedious preliminary tests. In addition, cell aging also deteriorates the accuracy of the EIS-based methods because the battery impedance deviates with the state of health [19], [20].

An alternative approach to estimate the core temperature is to build an observer based on the thermal–electrical model of lithium-ion batteries [21]–[25]. A lumped thermal–electrical model, whose thermal dynamics are defined by the surface and core temperatures, is usually utilized for core temperature estimation due to its simplicity and enough accuracy [25]–[29]. The thermal parameters are identified by the recursive least square (RLS) method based on the preliminary test data [21]. By utilizing the feedbacks of the surface temperature, cell voltage, and current, different model-based core temperature observers are built and proposed for real-time applications [21]–[25]. To deal with the time-varying model parameters, such as the temperature-dependent internal resistance, the Kalman filter (KF) is proposed to improve the accuracy of the core temperature estimation [23]–[25].

Nevertheless, both categories of the core temperature estimation methods are not applicable to the rapid self-heating cases. For the consideration of compactness, the onboard self-heating ac frequency is relatively high, at several kilohertz or more, to reduce the size of passive components. To extract the impedance information from the sampled ac heating current and cell voltage data, the EIS-based methods require a very high sampling rate to several hundred kilohertz, which is impractical for a real battery management system (BMS). Also, the shortage of battery current and voltage information caused by the low BMS sampling rate makes it difficult to estimate the heat generation rate in the thermal–electrical model-based methods [21]–[25]. These KF-based estimation methods are infeasible in self-heating applications due to the lack of the heat generation rate, which is not a Gaussian random process with zero mean. Therefore, the real-time tracking error of those core temperature estimation methods is not negligible during the self-heating, producing improper feedbacks to the BMS.

The main innovation of this article is to develop a feasible core temperature estimation method for the onboard battery self-heating application. The proposed method is based on the lumped thermoelectric model, where the time-invariant thermal resistances and capacities can be identified in advance. To cope with the model uncertainties and time-variant parameters in the estimation model, an extended state observer (ESO) with the feedback of the surface temperature is built to improve the estimation accuracy and guarantee the dynamic performance of the system. By properly tuning the parameters, the proposed ESO can adequately compensate for the influence of the temperature-dependent internal resistance, the open-circuit voltage, and other parameter uncertainties. Therefore, the core temperature can be accurately estimated within a short time during the onboard self-heating.

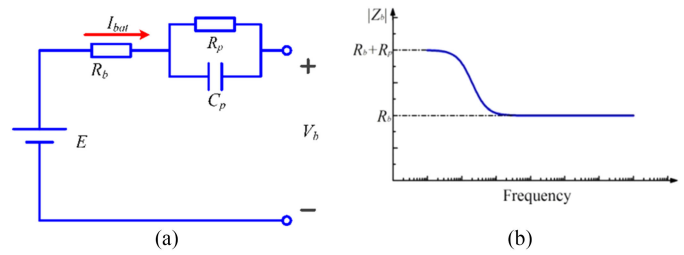


Fig. 1. Lithium-ion battery model. (a) Equivalent circuit model. (b) Equivalent internal impedance.

The primary benefit of the proposed method is to avoid the high-frequency current and voltage measurement for online estimation of battery impedance, because the proposed ESO is able to calibrate the estimated heat generation rate. With this method, the low-sampling-rate BMS is capable of estimating the core temperature in real time for the high-frequency self-heaters. The experimental results on 18 650 cells demonstrate that the proposed method can accurately estimate the core temperature without the information of the internal resistance during the short self-heating period. As a result, the core temperature monitoring helps reduce 50% of the heating time and energy consumption, leading to extended EV ranges

## II. SELF-HEATER FOR AUTOMOTIVE LITHIUM-ION BATTERIES

### A. Equivalent Circuit Model of the Lithium-Ion Battery

The onboard self-heater utilizes the internal resistance of lithium-ion batteries to generate the Joule heat for preheating. Thus, the electrical model of the lithium-ion battery is first established. From [30], it is known that the first-order  $RC$  model presented in Fig. 1(a) is widely used for its simplicity and acceptable precision in representing the lithium-ion battery dynamics. The equivalent impedance of this model can be expressed as

$$Z_b = R_b + \frac{R_p}{1 + \omega^2 R_p^2 C_p^2} - j\omega \frac{R_p^2 C_p}{1 + \omega^2 R_p^2 C_p^2} \quad (1)$$

where  $R_b$  denotes the ohmic resistance.  $R_p$  and  $C_p$  are the polarization resistance and capacitance, respectively. According to (1), the battery impedance is almost equal to  $R_b$  under high-frequency excitations, as shown in Fig. 1(b). Since the self-heating current is usually at a high frequency such as 10 kHz or more, it is accurate enough to only take  $R_b$  to calculate the Joule heat generation  $Q_b$ , e.g.,  $Q_b = I_b^2 R_b$ .

### B. Self-Heater for Automotive Lithium-Ion Batteries

The proposed onboard self-heater is based on the inductor ladder topology, as shown in Fig. 2(a). The terminals of the battery pack are connected to the power switches, and the midpoint of the series cell string is connected to the inductors. In the interleaved structure, the energy can be transferred from the upper battery strings to the lower ones, and *vice versa*. Therefore, the ac heating current can be generated by the proposed self-heater without external power supplies.

The pulsewidth modulation (PWM) signals for power switches  $S_1$  ( $S_3$ ) and  $S_2$  ( $S_4$ ) are complementary, and the duty

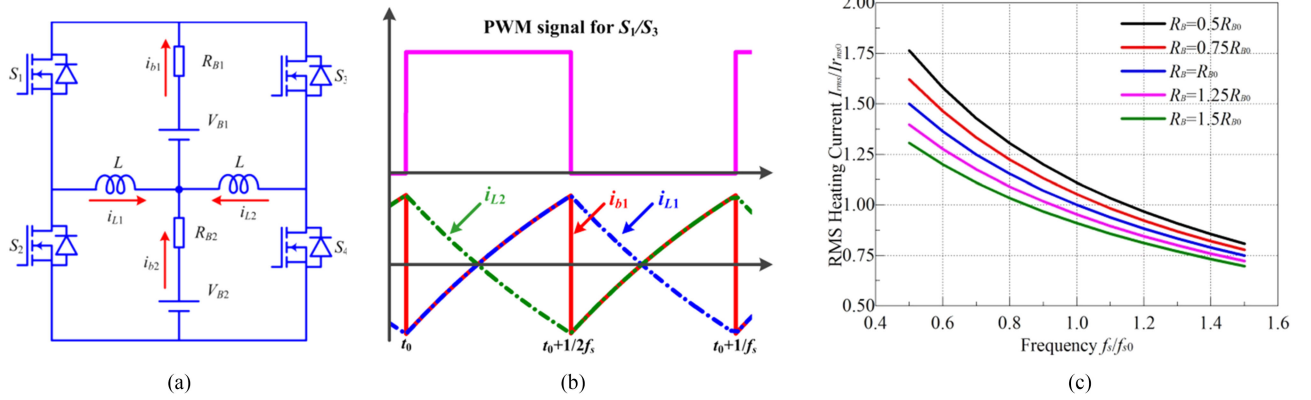


Fig. 2. Proposed onboard self-heater. (a) Circuit topology. (b) Waveforms. (c) RMS heating current with different internal resistance and switching frequencies.

ratios are 50% if neglecting the deadtime, as shown in Fig. 2(b). Assuming the battery cells have the same voltage and resistance, i.e.,  $V_{B1} = V_{B2} = V_B$ , and  $R_{B1} = R_{B2} = R_B$ , the battery heating currents  $i_{b1}$  and  $i_{b2}$  are symmetrical, as well as the inductor currents  $i_{L1}$  and  $i_{L2}$ . For example, the inductor current  $i_{L1}$  increases when  $S_1$  and  $S_3$  are turned ON. Considering the switching frequency is  $f_s$ ,  $i_{b1}$  during this period ( $t_0 \sim t_0 + 1/2 f_s$ ) can be expressed as

$$i_{b1}(t) = i_{L1}(t) = \frac{V_B}{2(R_B + R_o)} \left[ 1 - 2e^{-\frac{R_B + R_o}{L}(t-t_0)} + e^{-\frac{R_B + R_o}{2Lf_s}} \right] \quad (2)$$

where  $R_o$  denotes the sum of the power switches' turn-ON resistance, the parasitic resistance of the inductors, etc. Due to the symmetrical topology, when  $S_2$  and  $S_4$  are turned ON,  $i_{b1}$  is equal to  $i_{L2}$  and is  $180^\circ$  lagged to  $i_{L1}$ . As  $i_{L1}$  and  $i_{L2}$  are complementary, the heating current frequency is twice of the switching frequency  $f_s$ . The RMS heating current can be calculated as

$$I_{b1} = \sqrt{f_s \int_0^{1/f_s} i_{b1}^2(t) dt} = \frac{V_B}{R_B + R_o} \times \sqrt{\frac{2e^{-\frac{R_B + R_o}{2Lf_s}} + e^{-\frac{R_B + R_o}{Lf_s}} + 1}{2} - \frac{2Lf_s}{R_B + R_o} \left(1 - e^{-\frac{R_B + R_o}{Lf_s}}\right)}. \quad (3)$$

From (3), both the battery internal resistance  $R_B$  and the switching frequency  $f_s$  affect the RMS heating current, as shown in Fig. 2(c). When  $R_B$  decreases with the rising core temperature during the self-heating, the RMS heating current increases even if  $f_s$  is constant. Therefore, the accurate value of the RMS current is not easy to obtain from the self-heating circuit model. Another approach to obtaining the RMS heating current is to directly sample and log the current waveforms for RMS calculation. However, the heating current frequency is several kilohertz. Thus, the required sampling rate for RMS calculation should be as high as several hundred kilohertz, which is not feasible for an onboard BMS. The low sampling rate also makes

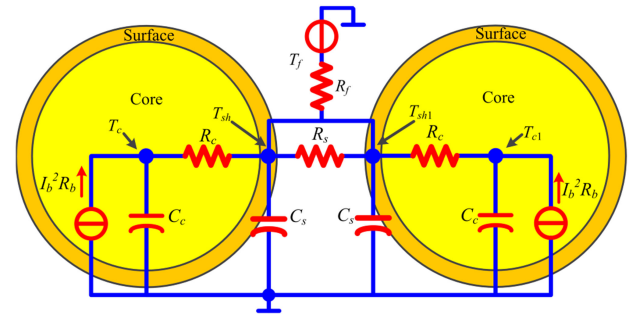


Fig. 3. Lumped two-layer thermal model of lithium-ion batteries.

the online EIS estimation impossible with the high-frequency current. Accordingly, neither the heat generation rate  $I_b^2 R_B$  nor the EIS characteristic is achievable during the self-heating. Therefore, both categories of the previous core temperature estimation methods in [18]–[20] and [21]–[25] are ineffective in self-heating applications. To solve this issue, a novel core temperature estimation method, operating without the precise information of the heat generation rate and the EIS characteristic, is introduced in detail in the next section.

### III. ONLINE CORE TEMPERATURE ESTIMATION

#### A. Lumped Thermal Model of the Lithium-Ion Battery

For the battery core temperature estimation, an accurate thermal model has to be established. In previous studies, plenty of thermal models are developed to describe the thermal dynamics of lithium-ion batteries. Among them, the partial differential equation-based thermal models can predict the detailed temperature distribution throughout the battery, whereas they are too complicated to compute in real time. Instead, single-state models, where a bulk temperature represents the thermal dynamic, have been used due to their computational efficiency. To balance the computational efforts and model accuracy, the lumped two-state thermal models are developed for capturing both the surface and the core temperatures [25]–[28]. Also, the thermal impact of adjacent cells in a battery pack is considered and modeled in [29], as shown in Fig. 3. The core temperature

estimation methods in [21]–[25] have also proved that the two-layer lumped thermal model can provide enough accuracy in presenting the battery's thermal characteristics without too much complexity. By assuming that both the battery surface and core temperature are both uniform, the lumped battery thermal model can be expressed as

$$\begin{bmatrix} \dot{T}_c \\ \dot{T}_{sh} \end{bmatrix} = \begin{bmatrix} -\frac{1}{R_c C_c} & \frac{1}{R_c C_c} \\ \frac{1}{R_f C_s} & -\frac{1}{R_f C_s} - \frac{1}{R_c C_s} \end{bmatrix} \begin{bmatrix} T_c \\ T_{sh} \end{bmatrix} + \begin{bmatrix} \frac{1}{C_c} & 0 & 0 & 0 \\ 0 & \frac{1}{R_f C_s} & \frac{1}{R_s C_s} & \frac{1}{R_s C_s} \end{bmatrix} \begin{bmatrix} I_b^2 R_b \\ T_f \\ T_{sh1} \\ T_{sh2} \end{bmatrix} \quad (4)$$

where  $T_{sh}$  denotes the surface temperature,  $T_c$  denotes the core temperature, and  $T_f$  is the ambient temperature.  $R_c$  is the thermal resistance across the core and the surface, and  $R_f$  is the thermal resistance between the surface and the environment.  $C_c$  and  $C_s$  are the battery internal and surface thermal capacity, respectively. To model the heat transferred from the adjacent cells in an automotive battery pack,  $R_s$  is used to represent the thermal resistance across the adjacent cells, and  $T_{sh1}$  and  $T_{sh2}$  are the adjacent cell temperatures. Due to the cells evenly distributed in a battery pack, the thermal resistances  $R_s$  across the adjacent cells are assumed to be equal. If the cell is located at the boundary of a pack, it is only affected by one side of the adjacent cell. By considering both the natural convection and the heat transferred from adjacent cells, the proposed thermal model is accurate enough for onboard applications. Note that the thermal parameters  $R_c$ ,  $R_s$ ,  $R_f$ ,  $C_c$ , and  $C_s$  are related to the battery materials and shape, and are assumed to be constant during the whole cycle life of the battery.  $I_b^2 R_b$  can represent the total heat generation rate during the high-frequency self-heating.

In order to estimate the core temperature with the proposed thermal model, the thermal parameters in (4) should be acquired. Authors in [21]–[25] described several practical parameter identification methods that can precisely obtain the thermal parameters after preliminary tests. In the case of self-heating, the constant parameters  $R_s$ ,  $R_c$ ,  $R_f$ ,  $C_s$ , and  $C_c$  can be identified by the RLS-based method in advance. However, due to the limitation of the sampling rate, the temperature-dependent resistance  $R_b$  and the RMS value of the high-frequency heating current are still unavailable by an onboard BMS.

### B. ESO for Internal Temperature Estimation

In previous methods, the KF or extended KF (EKF) is used to estimate the core temperature and other battery states [21]–[25]. In such cases, the low-frequency battery current can be measured by the BMS directly, as well as the terminal voltage. Based on the circuit model of the battery, the internal resistance can be identified online by using the measured current and voltage. Then, the heat generation rate  $I_b^2 R_b$  can be easily obtained to estimate the core temperature.

However, in the self-heating applications, the KF-based observer cannot be used directly due to the absence of the battery current and resistance information. In this article, an estimation strategy based on the ESO is proposed for the core temperature estimation in the self-heating application. The ESO was developed to deal with the control problems with unknown parameters or parameter uncertainties [31].

The inaccurate estimated RMS heating current and internal resistance can be represented by  $\hat{I}_b$  and  $\hat{R}_b$ , respectively. The system disturbance caused by the uncertain parameters is expressed by  $d = I_b^2 R_b - \hat{I}_b^2 \hat{R}_b$ . Hence, the estimation accuracy of the core temperature is significantly affected by the parameter uncertainties of  $I_b$  and  $R_b$  in the self-heating cases.

Since the core temperature dynamic is dependent on  $d$ , it can be modeled as an augmented state. By assuming  $h$  as the derivative of  $d$ , the battery thermal model considering the inaccurate parameters and uncertain input can be augmented and expressed as

$$\begin{bmatrix} \dot{T}_c \\ \dot{T}_{sh} \\ \dot{d} \end{bmatrix} = \begin{bmatrix} -1/R_c C_c & 1/R_c C_c & 1 \\ 1/R_f C_s & -1/R_f C_s - 1/R_c C_s & 0 \\ 0 & 0 & 0 \end{bmatrix} \begin{bmatrix} T_c \\ T_{sh} \\ d \end{bmatrix} + \begin{bmatrix} 1/C_c & 0 & 0 & 0 \\ 0 & \frac{1}{R_f C_s} & \frac{1}{R_s C_s} & \frac{1}{R_s C_s} \\ 0 & 0 & 0 & 0 \end{bmatrix} \begin{bmatrix} \hat{I}_b^2 \hat{R}_b \\ T_f \\ T_{sh1} \\ T_{sh2} \end{bmatrix} + \begin{bmatrix} 0 \\ 0 \\ h \end{bmatrix}. \quad (5)$$

As the only measurable state in (5) is the surface temperature  $T_{sh}$ , it can be seen as the system output. Thus, the two-layer thermal model with uncertainties can be rewritten as

$$\begin{cases} \dot{x} = \mathbf{A}x + \mathbf{B}u + \mathbf{E}h \\ y = \mathbf{C}x \end{cases} \quad (6)$$

where

$$\mathbf{A} = \begin{bmatrix} -\frac{1}{R_c C_c} & \frac{1}{R_c C_c} & 1 \\ \frac{1}{R_f C_s} & -\frac{1}{R_f C_s} - \frac{1}{R_c C_s} & 0 \\ 0 & 0 & 0 \end{bmatrix}, \quad \mathbf{B} = \begin{bmatrix} \frac{1}{C_c} & 0 & 0 & 0 \\ 0 & \frac{1}{R_f C_s} & \frac{1}{R_s C_s} & \frac{1}{R_s C_s} \\ 0 & 0 & 0 & 0 \end{bmatrix},$$

$$\mathbf{C} = [0 \ 1 \ 0], \mathbf{E} = \begin{bmatrix} 0 \\ 0 \\ 1 \end{bmatrix}, x = \begin{bmatrix} T_c \\ T_{sh} \\ d \end{bmatrix}, u = \begin{bmatrix} \hat{I}_b^2 \hat{R}_b \\ T_f \\ T_{sh1} \\ T_{sh2} \end{bmatrix}.$$

The observability matrix  $\mathbf{Q}_o$  of the augmented system in (6) can be calculated by (7), shown at the bottom of the next page.

As all the thermal parameters in  $\mathbf{Q}_o$  are positive, the rank of  $\mathbf{Q}_o$  is 3 apparently, so that the augmented system is observable. By assuming the observed state  $\hat{x} = [\hat{T}_c \hat{T}_{sh} \hat{d}]^T$ , the ESO can be built according to the principle presented in [28]

$$\dot{\hat{x}} = \mathbf{A}\hat{x} + \mathbf{B}u + \mathbf{L}(y - \mathbf{C}\hat{x}) \quad (8)$$

where  $\mathbf{L} = [\beta_1 \beta_2 \beta_3]^T$  is the observer gain. From (8), it is clear that the battery surface temperature  $T_{sh}$  is utilized as the feedback state to calibrate the observer output.

Due to the presence of the integral item of the observation error, the ESO performs like a PID controller to eliminate the disturbances in the loop. Therefore, even if the internal resistance  $R_b$  and RMS heating current  $I_b$  are not precisely obtained during the self-heating, the feedback of  $T_{sh}$  can well calibrate and estimate the heat generation rate due to the augmented system disturbance state  $d$ . Therefore, the proposed ESO in (8) can accurately estimate the core temperature when the estimated surface temperature  $\hat{T}_{sh}$  converges to the real value  $T_{sh}$ . It should be noted that the proposed ESO-based estimation method only needs the surface temperature feedback with the preacquired thermal parameters. Hence, this method can also be implemented for other heating topologies and applications.

### C. Observer Gain Design Principle for the ESO

Due to the short duration time of the self-heating, the core temperature observer should provide fast dynamic performance. Consequently, the observer gain  $\mathbf{L}$ , which determines the dynamic performance and the stability margin of the ESO, should be carefully designed. In this article, the design method for the observer gains is introduced to provide satisfying performance in self-heating applications.

According to the design principle in [31], the characteristic equation of the observer system presented by (8) can be represented by

$$\begin{aligned} |sI - A| &= s^3 + \left( \frac{1}{R_c C_c} + \frac{1}{R_c C_s} + \frac{1}{R_s C_s} + \beta_2 \right) s^2 \\ &+ \frac{1}{R_c^2 C_c C_s} \left( \frac{1}{R_c C_s} + \frac{1}{R_s C_s} + \beta_2 \right) \left( \beta_1 - \frac{1}{R_c C_c} \right) s \\ &+ \frac{\beta_3}{R_c C_s}. \end{aligned} \quad (9)$$

In order to balance the system dynamic and stability performance, the observer gains are adjusted so that the observer has three identical poles [31], e.g.

$$|sI - A| = (s + \omega_n)^3 \quad (10)$$

where  $\omega_n$  is the designed triple pole and the bandwidth of the observer as well. By substituting (10) into (9), the observer gains

can be expressed as

$$\begin{cases} \beta_1 = \frac{2R_c^3 C_c^2 C_s \omega_n^2}{2R_c C_c \omega_n - 1} + \frac{1}{R_c C_c} \\ \beta_2 = 2\omega_n - \frac{1}{R_c C_c} - \frac{1}{R_c C_s} - \frac{1}{R_s C_s} \\ \beta_3 = R_c C_s \omega_n^3 \end{cases} \quad (11)$$

From (11), it is clear that the observer gains are determined by the observer bandwidth  $\omega_n$ . Therefore,  $\omega_n$  should be determined first. Basically, a high observer bandwidth is preferred in self-heating cases to capture the core temperature dynamics. However, in the digital control domain, the observer bandwidth  $\omega_n$  is constrained by the sampling frequency of the BMS, which is usually set to be lower than 1/10 of the sampling rate to guarantee the loop stability.

Another constraint of the observer gain is that  $\beta_1$ ,  $\beta_2$ , and  $\beta_3$  should be all positive to guarantee the observer system stability. Based on (10), the extra limitation of  $\omega_n$  can be solved as

$$\begin{cases} \omega_n > \frac{1}{2R_c C_c} \\ \omega_n > \frac{1}{2R_c C_c} + \frac{1}{2R_c C_s} + \frac{1}{2R_s C_s} \\ \omega_n > 0 \end{cases} \quad (12)$$

From (12), it is obvious that  $\omega_n$  should be larger than  $1/2R_c C_c + 1/2R_c C_s + 1/2R_s C_s$  to form the negative feedback of the surface temperature  $T_{sh}$  in the ESO.

Equation (12) illustrates that the system stability is deteriorated if a too low bandwidth is implemented. Therefore, the bandwidth  $\omega_n$  of the ESO should be

$$\frac{1}{2R_c C_c} + \frac{1}{2R_c C_s} + \frac{1}{2R_s C_s} < \omega_n < \frac{2\pi f_s}{10} \quad (13)$$

where  $f_s$  is the temperature sampling rate. After determining the bandwidth  $\omega_n$ , the ESO gains can be calculated from (11).

It should be noted that the KF-based observer can also be implemented in the augmented system of (6) for core temperature estimation. The only difference from the proposed ESO is that the observer gain  $\mathbf{L}$  in the KF-based observer is iteratively calculated and time variant in each step. However, there are complicated matrix inverse calculations in the KF-based observer. For simplicity and real-time capability, the proposed ESO is preferred for onboard implementation and also provides satisfactory performance, which will be demonstrated in the next section.

## IV. EXPERIMENTAL VALIDATION

The test bench of the buck-boost converter-based self-heater is built. The experimental system setup is depicted in Fig. 4.

$$\mathbf{Q}_o = \begin{bmatrix} \mathbf{C} \\ \mathbf{C} \cdot \mathbf{A} \\ \mathbf{C} \cdot \mathbf{A} \cdot \mathbf{A} \end{bmatrix} = \begin{bmatrix} 0 & 1 & 0 \\ 1/R_f C_s & -1/R_f C_s - 1/R_c C_s & 0 \\ -(1/R_c C_s + 1/R_f C_s + 1/R_c C_c)/R_f C_s & (1/R_c C_s + 1/R_f C_s)^2 + 1/R_c R_f C_c C_s & 1/R_f C_c C_s \end{bmatrix} \quad (7)$$

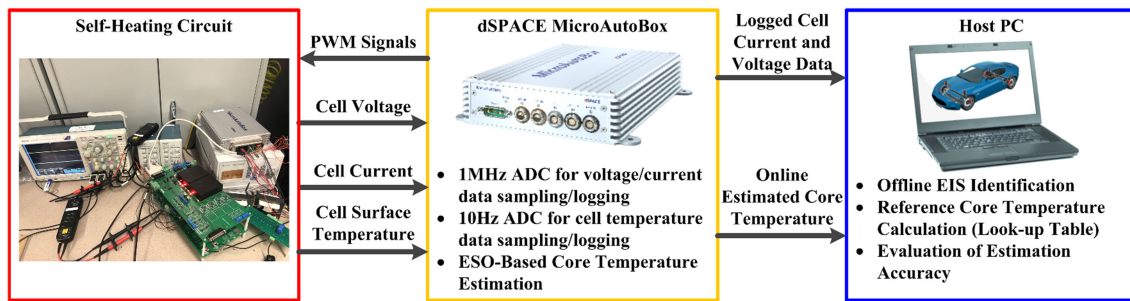


Fig. 4. Experimental setup of the proposed battery self-heater and core temperature estimation.

Inductances of  $L_1$  and  $L_2$  in the circuit are  $22 \mu\text{H}$ . The BMS is emulated by a dSPACE MicroAutoBox processor with 10-Hz sampling frequency for the cell temperature. Two additional 1-MHz ADC channels are used to record the current and voltage waveforms for offline impedance analysis, which will be discussed later on. For simplicity and generality, six 2500 mAh 18 650 LiNiMnCoO<sub>2</sub> cells are connected in series to emulate an automotive battery pack. The surface temperature is measured via K-type thermocouples attached to the battery cells.

### A. Thermal Parameter Identification

Before the core temperature estimation, the thermal parameters of the 18 650 cells need to be identified. The urban dynamometer driving schedule (UDDS) test cycle for the batteries is performed for four times in a row by the Arbin Battery Tester. As shown in Fig. 5(a) and (b), the battery voltage, current, and temperature are recorded and used for parameter estimation. According to [21], the thermal capacities  $C_c$  and  $C_s$  of the cylindrical cell can be empirically set to 45 and 3.2 J/W, respectively. Then, by implementing the RLS-based method in [21], the thermal resistances  $R_c$ ,  $R_f$ , and  $R_s$  can be identified, which converge to 3.2, 5.1, and 25.2 K/W in the identification, as shown in Fig. 5(c). It should be noted that  $R_s$  is much larger than  $R_c$  and  $R_f$ , denoting that the thermal impact of adjacent cells is minor. Therefore, the boundary effect of the temperature distribution is not obvious in the tested cells. The reason is that the gaps between the adjacent cells are almost 1.5 cm in the proposed experimental setup. However, in a real battery pack, the thermal resistance across the adjacent cells should be small, because the cells are located closely.

### B. Measurement of Impedance–Temperature Curve

Since it is difficult to install the thermocouples inside the cylindrical 18 650 cells, the direct measurement of the core temperature for validation becomes inaccessible. In this article, we use the measured EIS to estimate the core temperature as the reference value. As the change in impedance with respect to SOC is negligible in the normal vehicle battery operation range (20–80% SOC), only the impedance–temperature characteristic has to be considered in the onboard cases [18]. The tested cells are soaked in a thermal chamber at various temperatures for 10 h, and the impedance–temperature curves at 80% SOC are obtained via the IVIUMnSTAT electrochemical analyzer under different ac excitation frequencies, as shown in Fig. 6. It should be noted that the preliminary EIS measurement results are obtained at

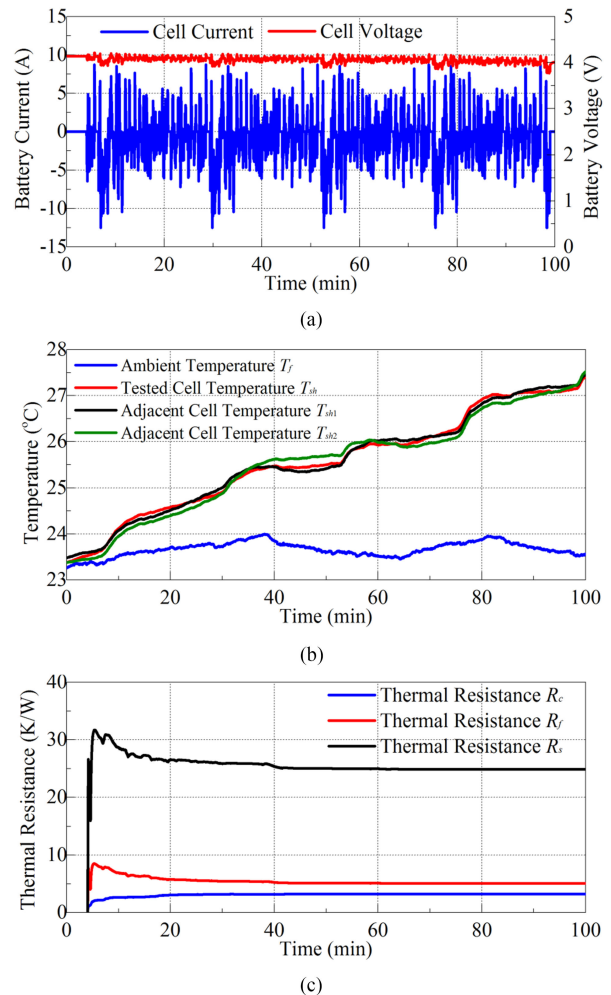


Fig. 5. Thermal parameter identification results. (a) Current and voltage. (b) Battery and ambient temperature. (c) Estimated thermal parameters.

uniform temperature distribution, while the battery cells are with the obvious temperature gradient during the self-heating. In [32] and [33], the theoretical and experimental analysis validates that the high-frequency EIS characteristic is only corresponding to the core temperature, while it is not likely to be affected by the temperature gradient. Therefore, the preliminary tested data can be implemented to compare with the measured battery impedance during the self-heating experiments to provide the reference core temperature.

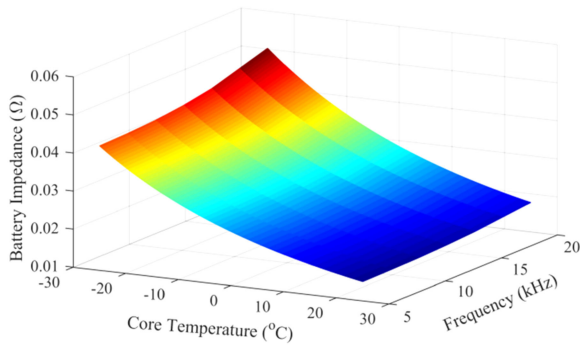


Fig. 6. Impedance–temperature characteristic of the tested 18650 cells under various ac excitation frequencies.

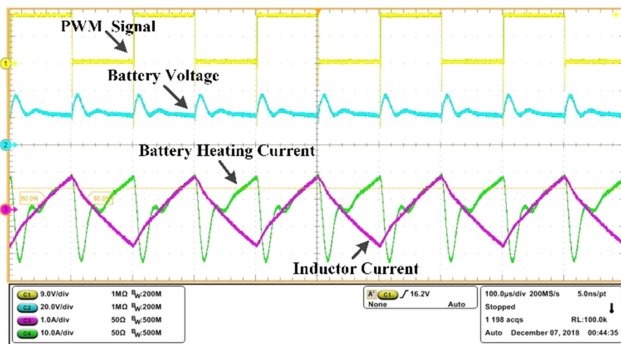


Fig. 7. Experimental waveforms of the proposed self-heater.

### C. Validation of the Proposed Self-Heater

Before the self-heating experiments, the tested cells are soaked to  $-20\text{ }^{\circ}\text{C}$  in a thermal chamber for 10 h. During the experiments, the setpoint of the thermal chamber is kept at  $-20\text{ }^{\circ}\text{C}$  to emulate a cold climate. The heating process ends when the surface temperature reaches  $0\text{ }^{\circ}\text{C}$ . The switching frequency of the self-heater varies from 3.5 to 5.5 kHz to obtain the 7–11 kHz heating currents, with the RMS value varying from 7.5 to 10 A (3C–4C).

The experimental waveforms are shown in Fig. 7. The high-frequency current is generated for preheating the cells. The RMS and average values of the heating current are calculated from the recorded current data. From Fig. 8(a) and (b), the RMS and average heating currents are relatively small at the initial heating stage and gradually enlarged with the rising temperature. It is caused by the reduced internal resistance during the self-heating and can be well explained by (3). With the 3C–4C RMS heating current, the battery surface temperature rapidly increases from  $-20$  to  $0\text{ }^{\circ}\text{C}$  by the proposed self-heater within 5.6–12.2 min, as shown in Fig. 9 (a).

### D. Core Temperature Estimation

The frequency of the cell current and voltage is around 10 kHz during the self-heating. To obtain the EIS of the tested cells, two ADC units operate at 1 MHz sampling rate to record the voltage and current data on the host PC. The proposed core temperature estimation is implemented during the self-heating experiments, in which the estimated core temperature values

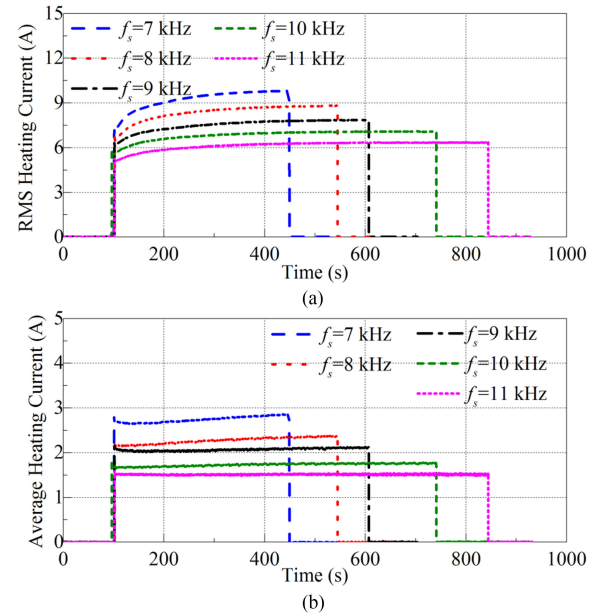


Fig. 8. Experimental results of the self-heating. (a) RMS heating current. (b) Average heating current.

are also recorded on the host PC. To evaluate the accuracy of the estimated core temperature, the reference core temperature is obtained through the EIS-based method. With the recorded cell voltage and current data during the self-heating, the battery impedance can be identified offline by conducting the algorithm in [18]. Based on the preliminary EIS–temperature curves shown in Fig. 6, the reference core temperature can be obtained offline and compared with the online estimation results for validating the proposed strategy. It should be noted that the onboard BMS is unable to provide such a high sampling rate, so that this EIS-based method is only feasible offline and on a specially designed platform to validate the proposed ESO-based method.

The proposed core temperature estimation is implemented during the self-heating experiments. According to (12) and the pre-estimated thermal parameters, the ESO bandwidth range is  $0.0337\text{ rad/s} < \omega_n < 6.28\text{ rad/s}$ . In this article, we set  $\omega_n$  as 3.14 rad/s. From (10), the ESO gains can be calculated as  $\beta_1 = 4490.4$ ,  $\beta_2 = 6.1$ , and  $\beta_3 = 307.1$  to tune the bandwidth to 3.14 rad/s. The internal resistance  $R_b$  is unknown before the tests and is set to 150 m $\Omega$  (three cells connected in series) in the proposed ESO. The RMS heating current is roughly calculated by (3) with a fixed predetermined  $R_B$  to estimate the heat generation rate in the observer. As shown in Fig. 9(a), the observed surface temperature can converge to the measured value very quickly. Therefore, the observed core temperature can be obtained, which is obviously higher than the surface temperature, as shown in Fig. 9(b). It can be seen that the core temperature exceeds  $10\text{ }^{\circ}\text{C}$  when the surface temperature reaches  $0\text{ }^{\circ}\text{C}$ . Compared to the reference core temperature obtained through the EIS-based method, the estimated core temperature is almost identical, with an error of less than  $0.6\text{ }^{\circ}\text{C}$ .

In order to prove the parameter robustness of the proposed ESO, the unknown battery resistance  $R_b$  is set to a wide range from 15 to 1500 m $\Omega$  in the ESO. The experimental results

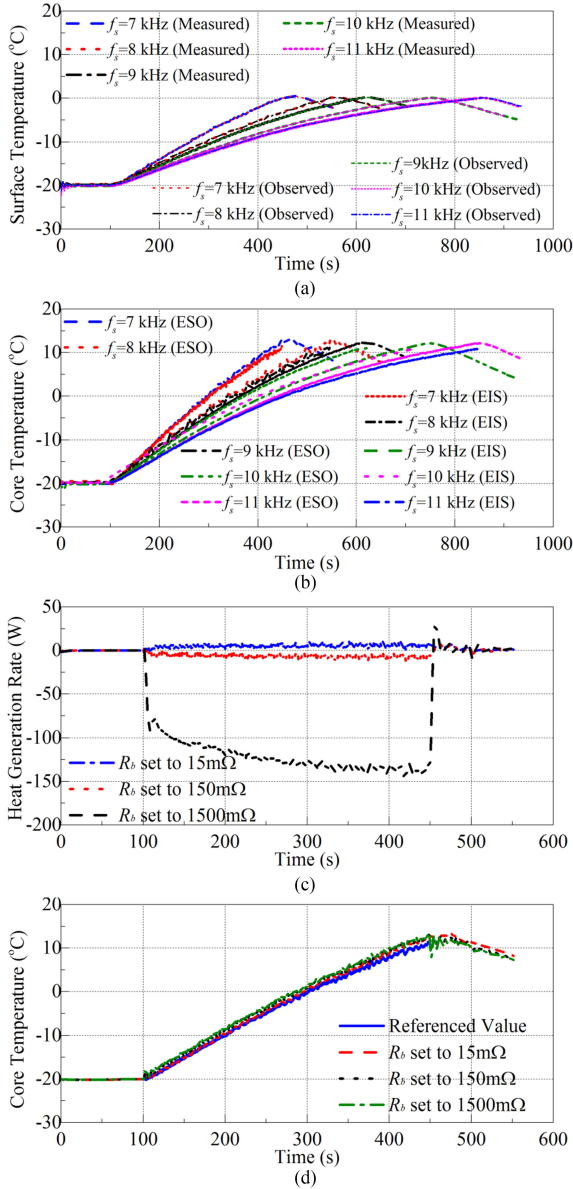


Fig. 9. Experimental results of the core temperature estimation. (a) Measured and observed surface temperatures. (b) Estimated core temperatures via the proposed ESO and the EIS-temperature characteristic. (c) Compensated heat generation rate under severe mismatch of  $R_b$ . (d) Estimated core temperatures under severe mismatch of  $R_b$ .

are presented in Fig. 9(c) and (d). It can be seen that the proposed ESO can compensate for the inaccurate heat generation rate  $d = I_b^2 R_b - \hat{I}_b^2 \hat{R}_b$  caused by the inaccurate resistance and heating current. Thus, even with the severe parameter error, the estimated error of the core temperatures is less than 1.2 °C at a substantially mismatched  $R_b$  of 1500 mΩ. The experimental results demonstrate that the proposed ESO has excellent compensation capability for battery parameter errors. Without any information on the battery impedance, the proposed core temperature estimation method still works well when the battery impedance changes gradually during the self-heating.

The temperature distribution of cells at different locations is also tested, as shown in Fig. 10. As expected above, the

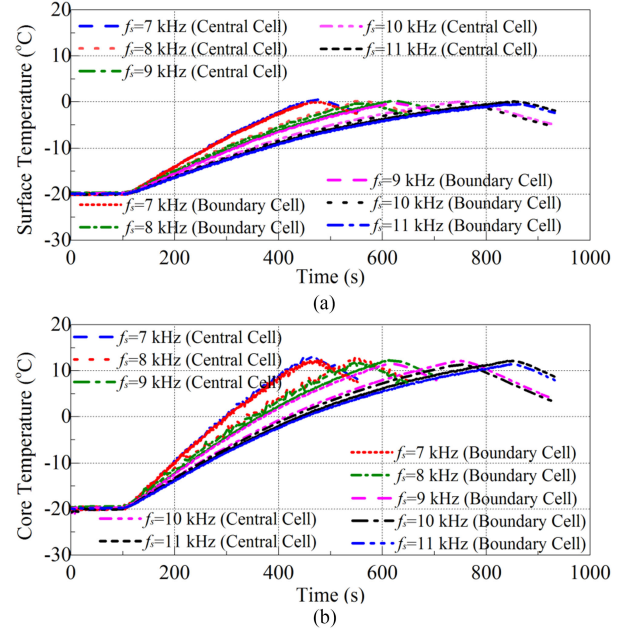


Fig. 10. Temperature distribution of the tested cells in a row. (a) Surface temperature. (b) Core temperature.

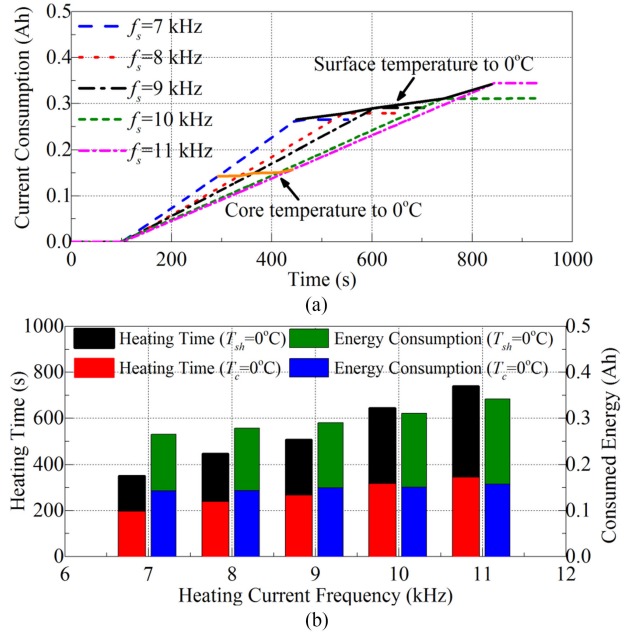


Fig. 11. Self-heating time and consumed energy in the experiments. (a) Amperé-hour curve. (b) Heating time and consumed energy.

experimental results show that the temperatures of the center-positioned cell and the boundary-positioned cell are of minor difference, because the thermal resistance  $R_s$  across the adjacent cells is relatively large in the proposed experimental setup. In a real battery pack, the boundary effect of the temperature distribution should be more evident with the closely placed cells.

As the core temperature is much higher than the surface temperature, the heating can be stopped when the core temperature reaches a preset threshold, thereby saving the heating time and energy in the self-heating. Fig. 11 shows the consumed battery

energy during the self-heating, which is acquired by using the ampere-hour integration on the average heating current. It can be concluded that the heating time and the consumed energy can be reduced by almost 50% by using the core temperature to monitor the self-heating. According to the experimental results, the proposed self-heater operating at 7 kHz only takes 193 s and 5.6% of the battery energy (0.14 C) to preheat the 18 650 cells from  $-20$  to  $0$  °C.

## V. CONCLUSION

In this article, an innovative core temperature estimation method was proposed for the onboard lithium-ion battery self-heating application. Based on the thermoelectric model of the lithium-ion battery, an ESO was built to estimate the core temperature during the self-heating. Due to the excellent uncertainty cancellation capability, the proposed ESO-based method could accurately estimate the core temperature during the battery self-heating.

Compared to previous core temperature estimation strategies, the precalibration of the impedance-temperature characteristic is no longer necessary, which saves testing time and cost, and excludes the estimation inaccuracy caused by the aging problems. Meanwhile, the heat generation rate can be calibrated by the ESO, so that the high-frequency sampling of the battery voltage and current can be eliminated with the ESO-based core temperature estimation. Therefore, the proposed method is particularly suitable for the onboard self-heating applications.

The experimental results show that the core temperature estimation error is within  $1.3$  °C even with severe parameter uncertainties, which is accurate enough for the self-heating applications. According to the core temperature estimation result, the heating time and energy consumption can be reduced by 50% compared with those of the surface-temperature-based heating strategy, which is beneficial for prolonging the available driving range of EVs in cold climates.

## REFERENCES

- [1] J. Zhang, L. Zhang, F. Sun, and Z. Wang, "An overview on thermal safety issues of lithium-ion batteries for electric vehicle application," *IEEE Access*, vol. 6, pp. 23848–23863, 2018.
- [2] S. Zhang, K. Xu, and T. R. Jow, "The low temperature performance of Li-ion batteries," *J. Power Sources*, vol. 115, no. 1, pp. 137–140, Mar. 2003.
- [3] S. Mohan, Y. Kim, and A. G. Stefanopoulou, "Energy-conscious warm-up of Li-ion cells from subzero temperatures," *IEEE Trans. Ind. Electron.*, vol. 63, no. 5, pp. 2954–2964, May 2016.
- [4] A. Pesaran, A. Vlahinos, and T. Stuart, "Cooling and preheating of batteries in hybrid electric vehicles," in *Proc. 6th ASME-JSME Therm. Eng. Joint Conf.*, 2003, pp. 1–7.
- [5] J. Jagemont, L. Boulon, Y. Dube, and F. Martel, "Thermal management of hybrid electric vehicle in cold weather," *IEEE Trans. Energy Convers.*, vol. 31, no. 3, pp. 1110–1120, Sep. 2016.
- [6] T. A. Stuart and A. Hande, "HEV battery heating using AC currents," *J. Power Sources*, vol. 129, pp. 368–378, Apr. 2004.
- [7] J. Zhang, H. Ge, Z. Li, and Z. Ding, "Internal heating of lithium-ion batteries using alternating current based on the heat generation model in frequency domain" *J. Power Sources*, vol. 273, pp. 1030–1037, Jan. 2015.
- [8] C.-Y. Wang *et al.*, "Lithium-ion battery structure that self-heats at low temperatures," *Nature*, vol. 529, no. 7587, pp. 515–518, Jan. 2016.
- [9] H. Ruan *et al.*, "A rapid low-temperature internal heating strategy with optimal frequency based on constant polarization voltage for lithium-ion batteries," *Appl. Energy*, vol. 177, pp. 771–782, Sep. 2016.
- [10] G. Zhang, S. Ge, T. Xu, X.-G. Yang, H. Tian, and C.-Y. Wang, "Rapid self-heating and internal temperature sensing of lithium-ion batteries at low temperatures," *Electrochim. Acta*, vol. 218, pp. 149–155, Nov. 2016.
- [11] Y. Shang, B. Xia, N. Cui, C. Zhang, and C. Mi, "An automotive onboard AC heater without external power supplies for lithium-ion batteries at low temperatures," *IEEE Trans. Power Electron.*, vol. 33, no. 9, pp. 7759–7769, Sep. 2018.
- [12] Y. Shang, C. Zhu, Y. Fu, and C. C. Mi, "An integrated heater-equalizer for lithium-ion batteries of electric vehicles," *IEEE Trans. Ind. Electron.*, vol. 66, no. 6, pp. 4398–4405, Jun. 2019.
- [13] H. Ruan *et al.*, "A low-temperature internal heating strategy without lifetime reduction for large-size automotive lithium-ion battery pack," *Appl. Energy*, vol. 230, pp. 257–266, Nov. 2018.
- [14] A. Hande, "Internal battery temperature estimation using series battery resistance measurements during cold temperatures," *J. Power Sources*, vol. 158, pp. 1039–1046, Aug. 2006.
- [15] J. P. Schmidt *et al.*, "Measurement of the internal cell temperature via impedance: Evaluation and application of a new method," *J. Power Sources*, vol. 243, pp. 110–117, Jun. 2013.
- [16] R. Srinivasan, B. G. Carkhuff, M. H. Butler, and A. C. Baisden, "Instantaneous measurement of the internal temperature in lithium-ion rechargeable cells," *IEEE Trans. Energy Convers.*, vol. 31, no. 3, pp. 1110–1120, Sep. 2016.
- [17] D. A. Howey, P. D. Mitcheson, V. Yufit, G. J. Offer, and N. P. Brandon, "Online measurement of battery impedance using motor controller excitation," *IEEE Trans. Veh. Technol.*, vol. 63, no. 6, pp. 2557–2566, Jul. 2014.
- [18] R. Richardson, P. Ireland, and D. Howey, "Battery internal temperature estimation by combined impedance and surface temperature measurement," *J. Power Sources*, vol. 265, pp. 254–261, Nov. 2014.
- [19] X. Hu, H. Yuan, C. Zou, Z. Li, and L. Zhang, "Co-estimation of state of charge and state of health for lithium-ion batteries based on fractional-order calculus," *IEEE Trans. Veh. Technol.*, vol. 67, no. 11, pp. 10319–10329, Nov. 2018.
- [20] Z. Wang, J. Ma, and L. Zhang, "State-of-health estimation for lithium-ion batteries based on multi-island genetic algorithm and Gaussian process regression," *IEEE Access*, vol. 5, pp. 21286–21295, 2017.
- [21] X. Lin *et al.*, "Online parameterization of lumped thermal dynamics in cylindrical lithium ion batteries for core temperature estimation and health monitoring," *IEEE Trans. Control Syst. Technol.*, vol. 21, no. 5, pp. 1745–1755, Sep. 2013.
- [22] C. Zhang, K. Li, and J. Deng, "Real-time estimation of battery internal temperature based on a simplified thermoelectric model," *J. Power Sources*, vol. 302, pp. 146–154, Jan. 2016.
- [23] H. Dai *et al.*, "Adaptive Kalman filtering based internal temperature estimation with an equivalent electrical network thermal model for hard-cased batteries," *J. Power Sources*, vol. 293, pp. 351–365, Oct. 2015.
- [24] C. Zhang, K. Li, J. Deng, and S. Song, "Improved real time state-of-charge estimation of LiFePO<sub>4</sub> battery based on a novel thermoelectric model," *IEEE Trans. Ind. Electron.*, vol. 64, no. 1, pp. 654–663, Jan. 2017.
- [25] Y. Kim, S. Mohan, J. B. Siegel, A. G. Stefanopoulou, and Y. Ding, "The estimation of temperature distribution in cylindrical battery cells under unknown cooling conditions," *IEEE Trans. Control Syst. Technol.*, vol. 22, no. 6, pp. 2277–2286, Nov. 2014.
- [26] X. Lin *et al.*, "A lumped-parameter electro-thermal model for cylindrical batteries," *J. Power Sources*, vol. 257, no. 15, pp. 1–11, Jul. 2014.
- [27] H. Perez, S. Dey, X. Hu, and S. Moura, "Optimal charging of Li-ion batteries via a single particle model with electrolyte and thermal dynamics," *J. Electrochem. Soc.*, vol. 164, no. 7, pp. A1679–A1687, 2017.
- [28] H. Perez, X. Hu, S. Dey, and S. Moura, "Optimal charging of Li-ion batteries with coupled electro-thermal-aging dynamics," *IEEE Trans. Veh. Technol.*, vol. 66, no. 9, pp. 7761–7770, Sep. 2017.
- [29] X. Lin *et al.*, "Parameterization and observability analysis of scalable battery clusters for onboard thermal management," *Oil Gas Sci. Technol.*, vol. 68, no. 1, pp. 165–178, Jan. 2013.
- [30] X. Hu, S. Li, and H. Peng, "A comparative study of equivalent circuit models for Li-ion batteries," *J. Power Sources*, vol. 195, no. 1, pp. 359–367, Jan. 2012.
- [31] S. Li, J. Yang, W. Chen, and X. Chen, "Generalized extended state observer based control for systems with mismatched uncertainties," *IEEE Trans. Ind. Electron.*, vol. 59, no. 12, pp. 4792–4802, Dec. 2012.
- [32] Y. Troxler *et al.*, "The effect of thermal gradients on the performance of lithium-ion batteries," *J. Power Sources*, vol. 247, no. 3, pp. 1018–1025, Feb. 2014.
- [33] H. Dai, B. Jiang, and X. Wei, "Impedance characterization and modeling of lithium-ion batteries considering the internal temperature gradient," *Energies*, vol. 11, no. 1, Jan. 2018, Art. no. 220.



**Chong Zhu** (M'17) received the B.S. degree from the China University of Mining and Technology, Xuzhou, China, in 2010, and the Ph.D. degree from Zhejiang University, Hangzhou, China, in 2016, both in electrical engineering.

He was a Postdoctoral Researcher with San Diego State University, San Diego, CA, USA, from 2017 to 2019. He is currently an Assistant Professor with the School of Mechanical Engineering, Shanghai Jiao Tong University, Shanghai, China. His research interests include battery thermal management, and design and control of power converters applied in electric vehicles.

research as a Joint Ph.D. Student with the Department of Electrical and Computer Engineering, San Diego State University, San Diego, CA, USA, where between December 2017 and January 2019, he was a Postdoctoral Research Fellow. His current research interests include battery balancing, self-heating for low-temperature batteries, battery modeling and states estimation, and design of battery management systems.



**Yunlong Shang** (S'14–M'18) received the B.S. degree in automation from the Hefei University of Technology, Hefei, China, in 2008, and the Ph.D. degree in control theory and control engineering from Shandong University, Shandong, China, in 2017.

In 2019, he joined Shandong University, where he is currently a Full Professor and Qilu Youth Talent Scholar with the School of Control Science and Engineering. Between September 2015 and October 2017, he conducted scientific

Dr. Shang was recipient of the Excellent Doctoral Dissertation Award of Chinese Association of Automation in 2018.



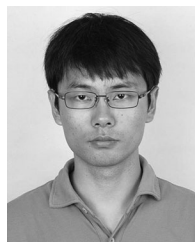
**Fei Lu** (S'12–M'17) received the B.S. and M.S. degrees from the Harbin Institute of Technology, Harbin, China, in 2010 and 2012, respectively, and the Ph.D. degree from the University of Michigan, Ann Arbor, MI, USA, in 2017, all in electrical engineering.

He is currently an Assistant Professor with the Department of Electrical and Computer Engineering, Drexel University, Philadelphia, PA, USA. His research interests include power electronics and the application of electric vehicle charging.



**Yan Jiang** was born in Jilin Province, China. He received the B.S. degree in electrical engineering and automation in 2014 from Beijing Jiaotong University, Beijing, China, where he is currently working toward the Ph.D. degree in electrical engineering.

He is currently with the National Active Distribution Network Technology Research Center, Beijing Jiaotong University. His research interests include battery state estimation, battery second use technology, and battery energy storage systems.



**Chenwen Cheng** received the B.S. and Ph.D. degrees in electrical engineering from Zhejiang University, Hangzhou, China, in 2012 and 2017, respectively.

He is currently a Postdoctoral Researcher with San Diego State University, San Diego, CA, USA. His research interests include the motor control, renewable power generation, and wireless power transfer technologies.



**Chris Mi** (S'00–A'01–M'01–SM'03–F'12) received the B.S.E.E. and M.S.E.E. degrees from Northwestern Polytechnical University, Xi'an, China, in 1985 and 1988, respectively, and the Ph.D. degree from the University of Toronto, Toronto, ON, Canada, in 2001, all in electrical engineering.

He is a Professor and the Chair of Electrical and Computer Engineering and the Director of the Department of Energy-funded Graduate Automotive Technology Education Center for Electric Drive Transportation, San Diego State University (SDSU), San Diego, CA, USA. Prior to joining SDSU, he was with the University of Michigan, Dearborn, MI, USA, from 2001 to 2015.